



High-Performance Rechargeable Lithium Batteries with Microspherated FeS₂ Cathode and Ether-based Electrolyte

Journal:	<i>Journal of Materials Chemistry A</i>
Manuscript ID:	TA-ART-03-2015-002169.R2
Article Type:	Paper
Date Submitted by the Author:	08-May-2015
Complete List of Authors:	Chen, Jun; Nankai Univ, Inst New Energy Mater Hu, Zhe; Nankai Univ, Key Lab Adv Energy Mat Chem Zhang, Kai; Nankai Univ, Zhu, Zhiqiang; Nankai Univ, Key Lab Adv Mater Energy Chem Tao, Zhanliang; Nankai Univ,

ARTICLE

FeS₂ Microspheres with Ether-based Electrolyte for High-Performance Rechargeable Lithium Batteries

Cite this: DOI: 10.1039/x0xx00000x

Zhe Hu¹, Kai Zhang¹, Zhiqiang Zhu¹, Zhanliang Tao¹, Jun Chen^{1,2*}Received 00th January 2012,
Accepted 00th January 2012

DOI: 10.1039/x0xx00000x

www.rsc.org/

Pyrite FeS₂ has been successfully applied in primary Li/FeS₂ batteries, but the poor cyclability in traditional carbonate-based electrolyte seriously hinders its application in rechargeable batteries. To overcome this issue, efforts have been done to focus on the modification of FeS₂. However, it is still difficult to improve the electrode performance especially for bare FeS₂. Herein, we report that changing carbonate-based electrolyte to selected ether-based lithium bis(trifluoromethanesulfonyl)imide and diglyme electrolyte greatly enhances the reversibility of the electrochemical reaction. FeS₂ microspheres with a high tap density of 2.2 g·cm⁻³ show the stable discharge capacities of 680 mAh·g⁻¹ at 100 mA·g⁻¹ and 412 mAh·g⁻¹ even at 6000 mA·g⁻¹. Moreover, the capacity retention is 90% after 100 cycles at 1000 mA·g⁻¹. The main reason for the long cycling is to inhibit the side reaction of the intermediate polysulfides with ether-based electrolyte.

Introduction

Batteries for electrochemical energy storage and conversion have become one of the most important devices in people's daily life.¹⁻⁵ As the technology development goes on, long life and high safety assurance become more and more important in designation of batteries.⁶⁻¹¹ However, the battery performance is mainly limited by the cathode material and thus reports focused on exploration of new materials and modification of existing materials are interesting.¹²⁻¹⁶ Pyrite FeS₂ as a classical cathode material creates great value in commercial primary lithium batteries by Energizer Company,¹⁷ mainly because of the cheap raw materials, abundant resources, and the capability of four-electron transfer (theoretical specific capacity of 893 mAh·g⁻¹). Meanwhile, researchers have tried intensive investigations on rechargeable Li/FeS₂ batteries, but still have to face the poor cycling of such batteries with common carbonate-based electrolyte (e.g. ethylene carbonate and diethyl carbonate (EC-DEC)).¹⁸

The electrochemical reactions of rechargeable Li/FeS₂ batteries are intercalation and conversion.¹⁹⁻²¹ During the discharge in the first cycle, FeS₂ reacts with Li to form Li₂FeS₂ with metallic conductivity,²² and then the conversion reaction with the formation of Fe metal and Li₂S happens. During the charge, partial S²⁻ is oxidized to S (always happening at ~2.3 V). Then in following cycles, the redox couple existing in Li/S batteries occurs. This couple generates polysulfides that would react with carbonate-based electrolyte as a side reaction (Fig. 1) and result in severe capacity loss and irreversible electrode

destruction during the cycles.²³⁻²⁷ Meanwhile, the huge volume change of phase transformation during repeated charge and discharge would result in the non-effective contact of the electrode materials, the inhomogeneous distribution of the electrolyte in the material surface/interface, and the polarization of the electrode.²⁸ This limits the application of FeS₂ as the cathode of rechargeable Li/FeS₂ batteries.

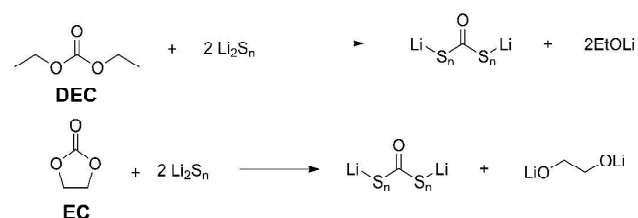


Fig. 1 The reaction between carbonate-based electrolyte (EC-DEC) and polysulfides.

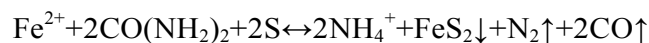
To improve the electrochemical performance of rechargeable Li/FeS₂ batteries, there are two efficient solutions. On one hand, much attention has focused on the modification of FeS₂ electrode.²⁹⁻³² Maier and co-workers found that by carbon compositing, carbon-encapsulated FeS₂ nanooctahedra greatly depressed the side reaction of FeS₂ with carbonate-based electrolyte.²⁹ The discharge capacity in LiPF₆/EC-DEC was 439 mAh·g⁻¹ at 1C and superior capacity retention of ~90% was kept at 0.5C after 50 cycles. On the other hand, it is found that electrolyte also plays a key role in determining the electrode

performance.³³ Yersak et al. obtained the improved discharge capacity of $750 \text{ mAh}\cdot\text{g}^{-1}$ at 0.1C and showed no obvious capacity fading after 20 cycles for rechargeable Li/FeS₂ batteries with solid state electrolyte.³¹ It is worth pointing out that ether-based electrolytes have recently been proved friendly to Li-S/Li-O₂ systems and also in Na/FeS₂ system.^{25, 34-37} This inspires us to carry out the study of using ether-based electrolyte to replace carbonate-based electrolyte on the effect of electrochemical performance of rechargeable Li/FeS₂ batteries. It is demonstrated that after optimization, ether-based electrolyte (lithium bis(trifluoromethanesulfonyl)imide (LiTFSI) and diglyme (DGM)) stabilizes the surface/interface of FeS₂ cathode. The assembled Li/FeS₂ batteries show the discharge capacity of $680 \text{ mAh}\cdot\text{g}^{-1}$ at $100 \text{ mA}\cdot\text{g}^{-1}$ and the capacity retention of 90% after 100 cycles at $1000 \text{ mA}\cdot\text{g}^{-1}$.

Experimental Section

Material synthesis

The FeS₂ microspheres were synthesized through a solvothermal method. 4 mmol FeSO₄·7H₂O, 20 mmol sublimed sulfur, and 20 mmol urea were dissolved into 70 mL of mixture of dimethyl formamide and ethylene glycol (4:3, v:v). Then, the suspension was under continuous stir and was transferred into 100 mL of Teflon-lined stainless steel autoclave and maintained at 180 °C for 8 h. Then FeS₂ was obtained:



The obtained product was centrifuged, washed with distilled water and absolute ethanol, and dried in the vacuum oven at 110 °C for 6 h.

Material Characterization

The crystalline structure of FeS₂ microspheres was proved by X-ray diffraction (XRD, Rigaku MiniFlex600, Cu K_α radiation). The morphology of FeS₂ was tested by scanning electron microscopy (SEM, JEOL JSM7500F) and high resolution transmission electron microscopy (HRTEM, Philips Tecnai F20). Raman spectra were characterized on a confocal Raman microscope (DXR, Thermo-Fisher Scientific) with an argon-ion laser ($\lambda=532 \text{ nm}$) in ambient air.

Electrochemical characterization

The electrochemical tests were measured via the CR2032 coin-type cells. The cathode electrode was consisted of 80% active materials, 10% KS-6 and 10% sodium carboxymethylcellulose (Na-CMC). The electrode materials was mixed by distilled water and coated onto the Cu current collector. The electrode was dried at 110 °C for 10 h in the vacuum oven and then pressed under 20 MPa by a tablet compression machine. Lithium foil was served as counter electrode and reference electrode, and glass fiber filter paper was used as the separator. The CR2032 coin cells were assembled in an argon-filled glove box. The electrolytes were 1.0 M lithium bis(trifluoromethanesulfonyl)imide (LiTFSI)

dissolved in diglyme (DGM) and 1.0 M LiPF₆ dissolved in the mixture of ethylene carbonate and diethyl carbonate (EC-DEC) with the volume ratio of 1:1. Galvanostatic charge/discharge tests were carried out on a Land CT2001A cell testing system. The cells were measured between 1.0–3.0 V vs. Li⁺/Li at various current densities. Cyclic voltammetry curves were measured with a Parstat 263A potentiostat/galvanostat workstation in the potential range of 1.0–3.0 V at $0.1 \text{ mV}\cdot\text{s}^{-1}$. Electrochemical impedance spectroscopy (EIS) was conducted on Parstat 2273 electrochemical workstation (AMETEK). The ac perturbation signal was $\pm 5 \text{ mV}$ and the frequency ranged from 100 mHz to 100 kHz.

Results

Fig. 2a shows the X-ray diffraction (XRD) pattern of the as-prepared FeS₂. The characteristic XRD peaks are in accordance with those of the cubic FeS₂ (standard JCPDS card No. 42-1340). The as-prepared FeS₂ belongs to the space group of Pa3. Fig. 2b and 2c exhibit the SEM images of as-prepared FeS₂ with two different magnifications. The SEM image in Fig. 2b shows the homogeneous distribution of FeS₂ microspheres. While, the SEM image in Fig. 2c displays that the microspheres are consisted of nanoplates. Because of the tightly assembled nanoplates, the integrated material gives a tap density of $2.2 \text{ g}\cdot\text{cm}^{-3}$, which provides high volumetric capacity to profit the practical applications. Fig. 2d shows the high resolution transmission electron microscope (HRTEM) image of the as-prepared FeS₂. The d-space of 0.27 and 0.24 nm corresponds to (200) and (210) lattice plane of FeS₂, respectively. The nitrogen adsorption-desorption isotherms are measured and placed in Fig. 2e. There is a hysteresis effect between the adsorption and desorption processes that is ascribed to the slit pores made by the accumulated nanoplates. The BET specific surface area is $28.9 \text{ m}^2\cdot\text{g}^{-1}$, which is good for the immersion of electrolyte. The Raman spectra are also tested (Fig. 2f). The peaks at around 373 cm^{-1} and 337 cm^{-1} represent the A_g and E_g vibration mode of FeS₂.³⁸ Moreover, the wider peaks of the as-prepared microspheres indicates smaller crystal size for the assembled nanoplates.³⁹

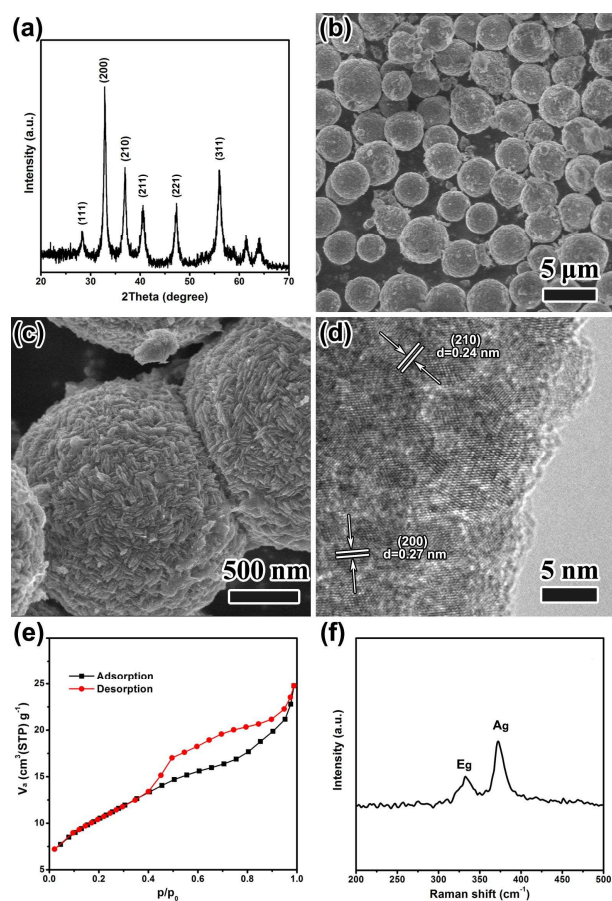
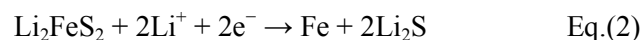


Fig. 2. (a) XRD pattern, (b,c) SEM images, and (d) HRTEM image, (e) N_2 adsorption and desorption isotherm, and (f) Raman shift of the as-prepared FeS_2 .

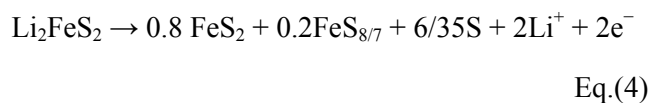
The electrochemical performance was tested in two electrolytes: ether and carbonate-ester. Here, we choose LiTFSI and DGM as the ether based electrolyte named Li/DGM, while $LiPF_6$ and EC-DEC as carbonate-based electrolyte named Li/EC-DEC. Fig. 3a and 3b show the galvanostatic profiles at the 1st, 5th, and 10th cycles. Cells in both kinds of electrolyte present two discharge platforms and two charge platforms in the initial cycle. Since FeS_2 microspheres were prepared in high purity (as demonstrated by XRD and Raman), the initial capacity of ~ 50 mAh/g above 1.7 V is attributed to the activation polarization, which is related to properties of electrolyte and electrode material.⁴⁰ By the way, the first discharge curve of FeS_2 anode materials of our work is similar to previous reports.^{29, 41} The discharge platforms at ~ 1.65 V and 1.45 V belong to the intercalation process of Li^+ (Eq. 1) and the conversion reaction (Eq. 2), respectively. It should be pointed out that the nanoplates assembled microspheres do good to the kinetics of first discharge process. The charge platforms at ~ 1.85 V and ~ 2.35 V are attributed to the electrochemical reaction (Eq. 3) and the oxidation of S^{2-} to S (Eq. 4), respectively.^{19, 20, 29, 31} At the following cycles, the platform around 2.3 V still exists in Li/EC-DEC indicating the continuous generation of polysulfides. However, the cell displays no obvious platform existing at ~ 2.3 V in charge process with Li/DGM, which means that no polysulfides is

generated, leading to stable cyclic performance. For FeS_2 microspheres with Li/DGM and Li/EC-DEC, the discharge capacities in the 1st cycle are $842 \text{ mAh}\cdot\text{g}^{-1}$ and $680 \text{ mAh}\cdot\text{g}^{-1}$, and the 10th discharge capacities are $683 \text{ mAh}\cdot\text{g}^{-1}$ and $85 \text{ mAh}\cdot\text{g}^{-1}$ at $100 \text{ mA}\cdot\text{g}^{-1}$, respectively. It is a very clear contrast that Li/DGM has play an important role in the cycling life as we make sure that all the other test parameters are controlled to be same.

Discharge:



Charge:



Moreover, the charge and discharge profiles are different from previous work by Choi et al.¹⁸ They used LiTFSI/TEGDME as the electrolyte, but the cell suffered from severe capacity fade due to the reason that the active cathode material is proved to be the mixture of marcassite FeS and pyrite FeS_2 . It should be pointed out that pure FeS has suffered more severe capacity fade during cycling.⁴² However, in this work, we synthesized pure FeS_2 microspheres assembled with nanoplates, producing the different charge and discharge profiles.

Fig. 3c and 3d show the CV data. Cell in Li/EC-DEC displays higher oxidation overpotential of ~ 0.15 V more than that in Li/DGM. During the following cycles, the voltage polarization in Li/EC-DEC gradually turns larger and the peak current decreases, meaning the capacity collapse (Fig. S1). In comparison, for the Li/DGM, the area under the curves tends to be stable, corresponding to the sustainable capacity. The narrow peaks also show that the cell with less polarization benefits from the fast kinetics. The reason why the inferior electrochemical performance happens in the cell with Li/EC-DEC is that sulfur generates at the fully charging state according to previous work.³⁰ While, at discharging process, sulfur turns into polysulfides that would react with the electrolyte leading to severe destruction of the active materials.^{23, 24} Thus, without efficient method like carbon-coating and solid-state electrolyte modification to protect sulfur from solving into the solvent, it is inevitable for pure FeS_2 cell to suffer severe capacity decay in traditional EC-DEC solvent.^{18, 29, 31, 43} However, Li-DGM electrolyte effectively inhibits the side reaction between polysulfides and electrolyte. Noting that no obvious reduction/oxidation peak in CV or platforms in galvanostatic curves above 2.0 V are found in the following cycles, which means no more S is generated in Li/DGM during the following charging.^{21, 44} This is responsible for the stable

discharge capacity and CV signal. Thus, the electrolyte optimization is necessary for Li/FeS₂ rechargeable batteries.

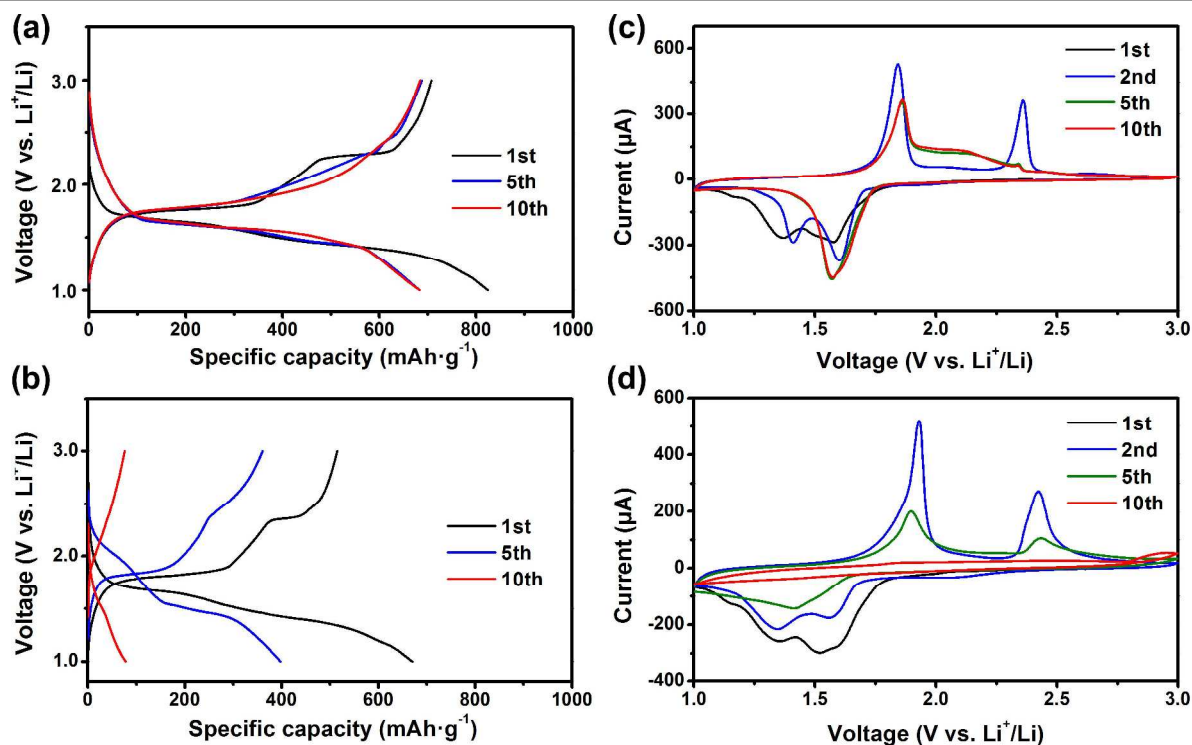


Fig. 3. Charge and discharge curves of FeS₂ microspheres in (a) Li/DGM and (b) Li/EC-DEC at current density of 100 mA·g⁻¹. CV curves in (c) Li/DGM and (d) Li/EC-DEC with a sweep rate of 0.1 mV·s⁻¹.

Electrochemical impedance spectroscopy (EIS) of the assembled cell with different electrolytes was characterized at the discharge platform around 1.65 V (Fig. 4a and 4b). At the 1st and 5th cycles, Li/DGM shows the similar semicircle, and both the data can be simulated by the equivalent circuit I (inset of Fig. 4a). The semicircle at high frequency is derived from the charge-transfer process (CPE_1 and R_{ct}), and the linear at low frequency is caused by the Li⁺ diffusion process (Z_w). However, the EIS data for Li/EC-DEC show different states between the 1st and 5th cycle (Fig. 4b). There is one semicircle at the 1st cycle, but two semicircles at the 5th cycle. As shown in the equivalent circuit II (inset of Fig. 4b), CPE_2 and R_s are corresponding to the high frequency semicircle with side reaction between the carbonate-ester and polysulfides on the interface of the electrode and electrolyte; While CPE_1 and R_{ct} generate the middle frequency semicircle. Detailed R_L , R_{ct} , and R_s are summarized in Table S1. The R_{ct} values also show that the charge-transfer resistance is decreasing from the 1st to the 5th cycle for both electrolytes. The R_{ct} is still smaller in Li/DGM than that of Li/EC-DEC, which reflects the out-performed kinetics in Li/DGM. From the above discussion, the EIS data changing in the Li/EC-DEC explains the side reaction occurring during cycling. On the contrary, the EIS data of the cell with Li/DGM expresses one semicircle all the time, and the R_{ct} value decreases with the cell cycling. This ensures the superior electrochemical performance. Furthermore, the ionic conductivity inside the crystal cell was calculated by using EIS data (Table S2). The Li⁺ diffusion efficiency is higher with

Li/DGM (2.9×10^{-10} cm²·s⁻¹) than that with Li/EC-DEC (1.6×10^{-10} cm²·s⁻¹). But they are almost in the same level. The reason is that Li⁺ ion travels inside the crystal cell as single ion but not solvent salt like Li/DGM or Li/EC-DEC. Thus, there is no significant difference between them.

The EIS data at different temperatures are also characterized (Fig. 4c and 4d). Increasing the temperature results in the decrease of the value of R_{ct} . At each temperature, R_{ct} is smaller in Li/DGM than that in Li/EC-DEC. The apparent activation energy was calculated by the Arrhenius equation:⁴⁵

$$i_0 = RT/nFR_{ct} \quad (\text{Eq. 5})$$

$$i_0 = A \exp(-E_a/RT) \quad (\text{Eq. 6})$$

where A is the temperature-independent coefficient, R is the gas constant, T is the absolute temperature, n is the number of transferred electrons, and F is the Faraday constant. The detailed E_a values are 38.1 kJ·mol⁻¹ and 51.4 kJ·mol⁻¹ for the cell with Li/DGM and Li/EC-DEC, respectively (Fig. 4e). The lower E_a for Li/DGM is responsible for the high capacity and preferred rate performance. The ionic conductivity of pure Li/DGM and Li/EC-DEC was measured (Fig. 4f). Li/DGM electrolyte displays higher ionic conductivity at all temperatures than that in Li/EC-DEC, meaning faster Li⁺ transportation in the electrolyte.

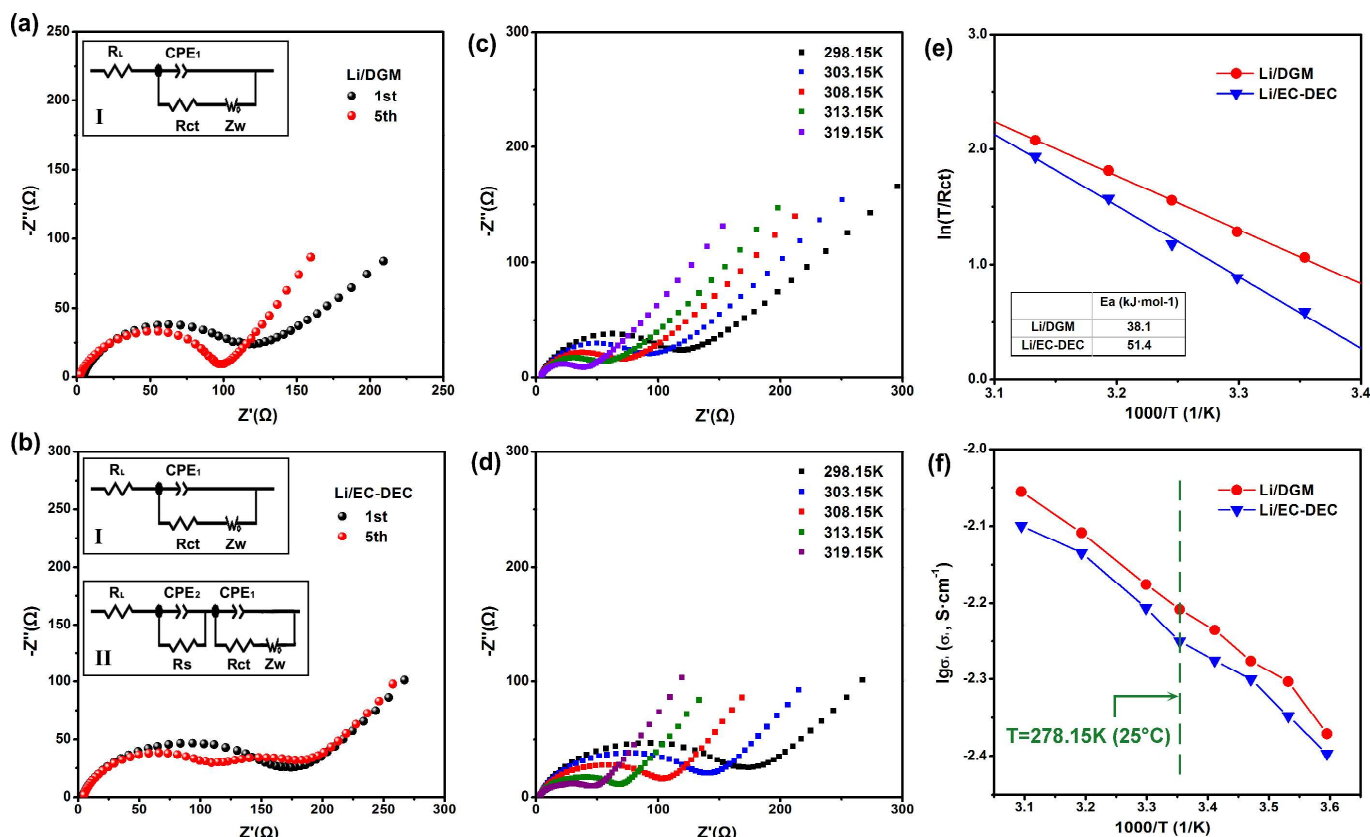


Fig. 4. Nyquist plots of EIS of as-prepared FeS₂ in (a) Li/DGM and (b) Li/EC-DEC at the platform around 1.65 V and 298 K in the 1st and 5th cycle. The Nyquist plots of FeS₂ microspheres in (c) Li/DGM and (d) Li/EC-DEC at different temperatures at the 1st discharge platform. (Each inset representing the equivalent circuit: R_L : the solution resistance; CPE_1 and CPE_2 : constant phase element of charge transfer and interface reaction, respectively; R_{ct} : charge transfer resistance; R_s : electrode surface reaction resistance; Z_w : Warburg resistance). (e) Arrhenius plots of $\ln(T/R_{ct})$ versus $1/T$ in Li/DGM and Li/EC-DEC (inset table displaying the detailed E_a value). (f) Ionic conductivity (σ) of Li/DGM and Li/EC-DEC at the selected temperatures from 278 K to 323 K.

Fig. 5 shows the electrochemical performances of FeS₂ microspheres in Li/DGM electrolyte. The charge/discharge curves in Fig. 5a show that the discharge capacities at the current density of 500, 1000, 2000, 3000, 4000, 5000, 6000, 7000, and 8000 mA·g⁻¹ are 615, 556, 521, 496, 465, 439, 412, 383, and 318 mAh·g⁻¹, respectively. As the active material loading is 1.2 mg·cm⁻², the current densities are 0.6, 1.2, 2.4, 3.6, 4.8, 6, 7.2, 8.4, and 9.6 mA·cm⁻², respectively. The capacity can return back to 549 mAh·g⁻¹ at 1000 mA·g⁻¹ (Fig. 5b). This indicates the recovery capability for FeS₂ microspheres to deal with high current density. Fig. 5c displays the Ragone plots of typical cathode materials in LIBs and FeS₂ microspheres in this work. The as-prepared FeS₂ possesses extremely high specific energy density of ~1000 Wh·kg⁻¹ (from Y axis), which is much higher than that of the optimized

LiNi_{0.5}Mn_{1.5}O₄, Li_{0.88}(Li_{0.18}Co_{0.33}Mn_{0.49})O₂, LiFePO₄, and LiMn₂O₄.⁴⁶⁻⁴⁹ Referring to the power density (from X axis), FeS₂ still shows comparable specific power density of 10,000 W·kg⁻¹ that ensures the possibility for fast charge and discharge in practical applications (The method shown in Supporting Information). However at high specific power, the FeS₂ decreases quickly because FeS₂ is not coated with carbon materials to obtain enough high electronic conductivity. In the future, we will try to prepare some FeS₂/carbon (like graphene) composites to improve this property. Cyclic performance is also tested to clarify the rechargeability of FeS₂ microspheres (Fig. 5d). The discharge capacities at 100th cycle with the current density of 1000 mA·g⁻¹ and 2000 mA·g⁻¹ are 540 mAh·g⁻¹ and 495 mAh·g⁻¹, showing the capacity retention of 90% and 85% (vs. the 2nd discharge capacity), respectively.

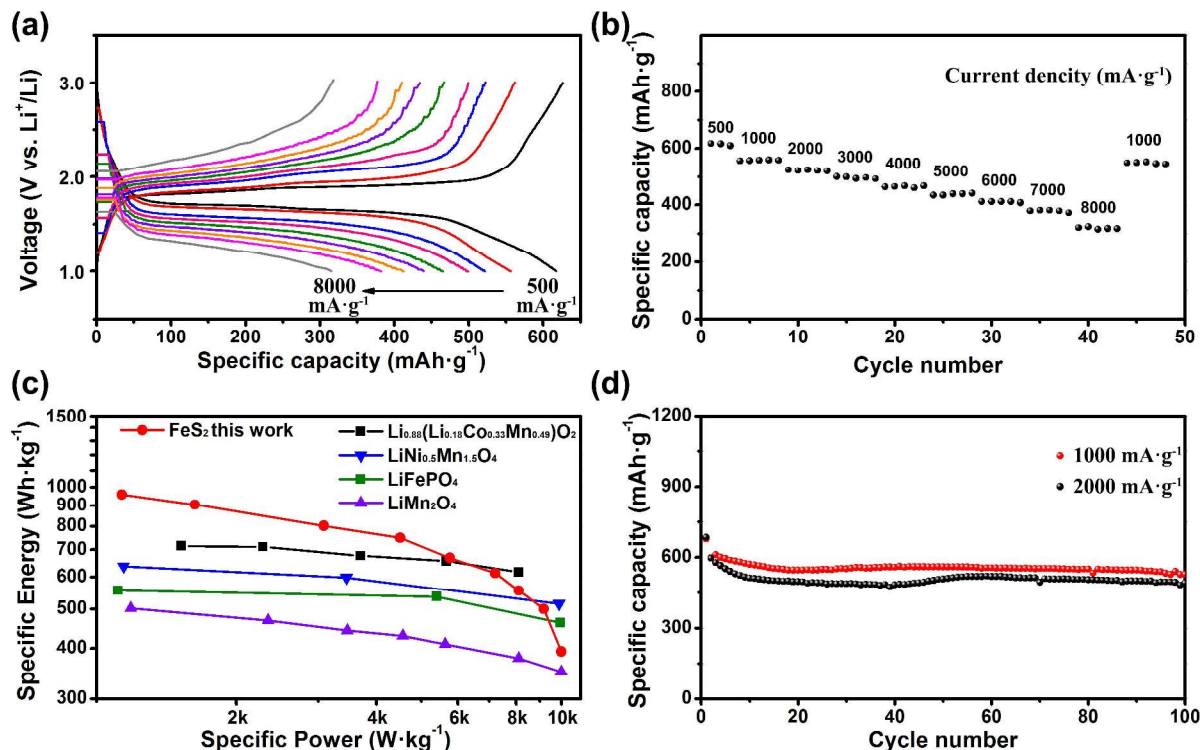


Fig. 5. (a) Charge and discharge curves of FeS₂/Li battery in Li/DGM at different current density (500 mA·g⁻¹ to 8000 mA·g⁻¹). (b) Rate performance in Li/DGM (the unit of current density is mA·g⁻¹). (c) Ragone plots of typical materials in LIBs and FeS₂ in this work. (d) Cyclic performance in Li/DGM at 1000 mA·g⁻¹ and 2000 mA·g⁻¹.

Conclusions

In summary, rechargeable Li/FeS₂ batteries with FeS₂ microspheres as the cathode and ether-based Li/DGM as the electrolyte show much better electrochemical performance than those with the Li/EC-DEC electrolyte. The main factor is that DGM largely inhibits both the generation of polysulfides and the side reaction between polysulfides and carbonate electrolyte. For the cells with Li/DGM electrolyte, the capacities of 680 mA·g⁻¹ at 100 mA·g⁻¹ and 412 mA·g⁻¹ at 6000 mA·g⁻¹ are obtained. Furthermore, the cells after cycling 100 times at 1000 mA·g⁻¹ and 2000 mA·g⁻¹ show the capacity retention of 90% and 85%, respectively. Our new results show that ether-based Li/DGM electrolyte is responsible for the much improved performance of carbon-free FeS₂. It also should be pointed out that the carbon-free Li/FeS₂ cell is able to serve as the rechargeable lithium batteries even in some extreme circumstance where high rate capability is emphasized, which shows more profit than the existing primary FeS₂ lithium batteries.

Acknowledgements

We acknowledge support from National 973 (2011CB935900), NSFC (21322101 and 21231005), and MOE (B12015, 113016A and ACET-13-0296).

Notes and references

¹Key Laboratory of Advanced Energy Materials Chemistry (Ministry of Education) and ²Collaborative Innovation Center of Chemical Science and Engineering, Nankai University, Tianjin, 300071, People's Republic of China. Fax: +86-22-23509571; Tel: +86-22-23506808; E-mail: chenabc@nankai.edu.cn.

Electronic Supplementary Information (ESI) available: [Cycling data, detailed EIS data, Li⁺ transfer coefficient, and calculation method for Power density and energy density] See DOI: 10.1039/c000000x/

1. M. Armand and J. M. Tarascon, *Nature*, 2008, **451**, 652.
2. H. Liu, D. Su, R. Zhou, B. Sun, G. Wang and S. Z. Qiao, *Adv. Energy Mater.*, 2012, **2**, 970.
3. J. Cabana, Z. Stoeva, J. J. Titman, D. H. Gregory and M. R. Palacin, *Chem. Mater.*, 2008, **20**, 1676.
4. Y. X. Wang, S. L. Chou, D. Wexler, H. K. Liu and S. X. Dou, *Chem. Eur. J.*, 2014, **20**, 9607.

5. Z. Hu, L. Wang, K. Zhang, J. Wang, F. Cheng, Z. Tao and J. Chen, *Angew. Chem. Int. Ed.*, 2014, **53**, 12794.
6. M. S. Islam and C. A. J. Fisher, *Chem. Soc. Rev.*, 2014, **43**, 185.
7. Z. W. Seh, H. Wang, N. Liu, G. Zheng, W. Li, H. Yao and Y. Cui, *Chem. Sci.*, 2014, **5**, 1396.
8. F. Cheng, J. Liang, Z. Tao and J. Chen, *Adv. Mater.*, 2011, **23**, 1695.
9. X. Han, T. Zhang, J. Du, F. Cheng and J. Chen, *Chem. Sci.*, 2013, **4**, 368.
10. K. Zhang, Z. Hu, Z. Tao and J. Chen, *Sci. China Mater.*, 2014, **57**, 42.
11. K. Zhang, Z. Hu, X. Liu, Z. Tao and J. Chen, *Adv. Mater.*, 2015, DOI:10.1002/adma.201500196.
12. B. L. Ellis, W. R. M. Makahnouk, Y. Makimura, K. Toghill and L. F. Nazar, *Nat. Mater.*, 2007, **6**, 749.
13. J. M. Clark, S. I. Nishimura, A. Yamada and M. S. Islam, *Angew. Chem. Int. Ed.*, 2012, **51**, 13149.
14. M. R. Jo, Y. I. Kim, Y. Kim, J. S. Chae, K. C. Roh, W. S. Yoon and Y. M. Kang, *Chem. Sus. Chem.*, 2014, **7**, 2248.
15. Y. Liang, P. Zhang and J. Chen, *Chem. Sci.*, 2013, **4**, 1330.
16. J. S. Chen and X. W. Lou, *Chem. Sci.*, 2011, **2**, 2219.
17. The website of Energizer Company is www.energizer.com.
18. J. W. Choi, G. Cheruvally, H. J. Ahn, K. W. Kim and J. H. Ahn, *J. Power Sources*, 2006, **163**, 158.
19. Y. Shao-Horn, S. Osmialowski and Q. C. Horn, *J. Electrochem. Soc.*, 2002, **149**, A1547.
20. R. Fong, J. R. Dahn and C. H. W. Jones, *J. Electrochem. Soc.*, 1989, **136**, 3206.
21. L. Li, M. Caban-Acevedo, S. N. Girard and S. Jin, *Nanoscale*, 2014, **6**, 2112.
22. Y. Yamaguchi, T. Takeuchi, H. Sakaebe, H. Kageyama, H. Senoh, T. Sakai and K. Tatsumi, *J. Electrochem. Soc.*, 2010, **157**, A630.
23. Y. X. Yin, S. Xin, Y. G. Guo and L. J. Wan, *Angew. Chem. Int. Ed.*, 2013, **52**, 13186.
24. J. Gao, M. A. Lowe, Y. Kiya and H. D. Abruña, *J. Phys. Chem. C*, 2011, **115**, 25132.
25. Z. Hu, Z. Zhu, F. Cheng, K. Zhang, J. Wang, C. Chen and J. Chen, *Energy Environ. Sci.*, 2015, **8**, 1309.
26. A. Manthiram, Y. Fu, S. H. Chung, C. Zu and Y. S. Su, *Chem. Rev.*, 2014, **114**, 11751.
27. T. Yim, M.-S. Park, J. S. Yu, K. J. Kim, K. Y. Im, J. H. Kim, G. Jeong, Y. N. Jo, S. G. Woo, K. S. Kang, I. Lee and Y. J. Kim, *Electrochimica Acta*, 2013, **107**, 454.
28. J. Xia, J. Jiao, B. Dai, W. Qiu, S. He, W. Qiu, P. Shen and L. Chen, *RSC Adv.*, 2013, **3**, 6132.
29. J. Liu, Y. Wen, Y. Wang, P. A. van Aken, J. Maier and Y. Yu, *Adv. Mater.*, 2014, **26**, 6025.
30. S. B. Son, T. A. Yersak, D. M. Piper, S. C. Kim, C. S. Kang, J. S. Cho, S. S. Suh, Y. U. Kim, K. H. Oh and S. H. Lee, *Adv. Energy Mater.*, 2014, **4**, 1300961.
31. T. A. Yersak, H. A. Macpherson, S. C. Kim, V. D. Le, C. S. Kang, S. B. Son, Y. H. Kim, J. E. Trevey, K. H. Oh, C. Stoldt and S. H. Lee, *Adv. Energy Mater.*, 2013, **3**, 120.
32. T. A. Yersak, C. Stoldt and S. H. Lee, *J. Electrochem. Soc.*, 2013, **160**, A1009.
33. E. Strauss, G. Ardel, V. Livshits, L. Burstein, D. Golodnitsky and E. Peled, *J. Power Sources*, 2000, **88**, 206.
34. Z. L. Wang, D. Xu, J. J. Xu and X. B. Zhang, *Chem. Soc. Rev.*, 2014, **43**, 7746.
35. Y. Yang, G. Zheng and Y. Cui, *Chem. Soc. Rev.*, 2013, **42**, 3018.
36. B. Jache and P. Adelhelm, *Angew. Chem. Int. Ed.*, 2014, **53**, 10169.
37. Q. Zhao, X. Hu, K. Zhang, N. Zhang, Y. Hu and J. Chen, *Nano Lett.*, 2015, **15**, 721.
38. A. M. Golsheikh, N. M. Huang, H. N. Lim, C. H. Chia, I. Harrison and M. R. Muhamad, *Chem. Eng. J.*, 2013, **218**, 276.
39. Y. Liang, R. Feng, S. Yang, H. Ma, J. Liang and J. Chen, *Adv. Mater.*, 2011, **23**, 640.
40. M. Winter and R. J. Brodd, *Chem. Rev.*, 2004, **104**, 4245.
41. X. Chen, Z. Wang, X. Wang, J. Wan, J. Liu and Y. Qian, *Inorg. Chem.*, 2005, **44**, 951.
42. L. Fei, Q. Lin, B. Yuan, G. Chen, P. Xie, Y. Li, Y. Xu, S. Deng, S. Smirnov and H. Luo, *ACS Appl. Mater. Interfaces*, 2013, **5**, 5330.
43. S. S. Zhang, *J. Mater. Chem. A*, 2015, **3**, 7689.
44. T. S. Yoder, M. Tussing, J. E. Cloud and Y. Yang, *J. Power Sources*, 2015, **274**, 685.
45. H. Gao, Z. Hu, K. Zhang, F. Cheng and J. Chen, *Chem. Commun.*, 2013, **49**, 3040.
46. Y. Lee, M. G. Kim and J. Cho, *Nano Lett.*, 2008, **8**, 957.
47. X. Zhang, F. Cheng, J. Yang and J. Chen, *Nano Lett.*, 2013, **13**, 2822.
48. B. Kang and G. Ceder, *Nature*, 2009, **458**, 190.
49. F. Cheng, H. Wang, Z. Zhu, Y. Wang, T. Zhang, Z. Tao and J. Chen, *Energy Environ. Sci.*, 2011, **4**, 3668.

TOC (no more than 20 words)

FeS₂ microspheres assembled with nanoplates show long cycling stability and high rate performance as the cathode of rechargeable Li batteries in optimized ether-based electrolyte.

